Environmental Science & Technology

pubs.acs.org/est

Article

Unexpected Gas-Phase Formation of Glycolic Acid Sulfate in the Atmosphere

Haowei Sun, Yuliang Liu,* Wei Nie,* Yuanyuan Li, Dafeng Ge, Tao Xu, Junchao Yin, Chong Liu, Zihao Fu, Ximeng Qi, Tengyu Liu, Qiaozhi Zha, Chao Yan, Zhe Wang, Xuguang Chi, and Aijun Ding

Cite This: *Environ. Sci. Technol.* 2025, 59, 16556−16566

Read Online

ACCESS | Metrics & More | Article Recommendations | Supporting Information

ABSTRACT: Organosulfates (OSs) are ubiquitous in atmospheric particulate matter and serve as key tracers of secondary organic aerosols. Traditionally, OSs have been primarily linked to the particle phase with their presence in the gas phase remaining largely undetected. This study provides compelling observational evidence of a continuously present gas-phase OS, glycolic acid sulfate (GAS), in an urban atmosphere using advanced mass spectrometry techniques. GAS concentrations exhibited distinct seasonal and diurnal patterns, peaking in summer with maximum levels of 4.6 × 10^4 cm^{-3} observed around midday, indicating a photochemical origin. Thermal desorption profile analysis revealed GAS as an extremely low-volatility organic compound, suggesting preferential aerosol partitioning. Remarkably, the observed gas-phase fraction of GAS exceeded predictions based on gas-particle equilibrium theory by 5−7 orders of magnitude, strongly suggesting the existence of a distinct source from gas-phase chemistry. We propose a potential formation mechanism involving the reaction between the SO_3 radical and glycolic acid (GA), which correlates nearly linearly with GAS production rates, suggesting a near-collision-limited rate constant ($k_{field} \approx 2.2 \times 10^{-10}$ cm^3 s^{-1}). This study fundamentally reshapes our understanding of OS sources and underscores the potential involvement of SO_3 in the formation of low-volatility organic compounds in the atmosphere.

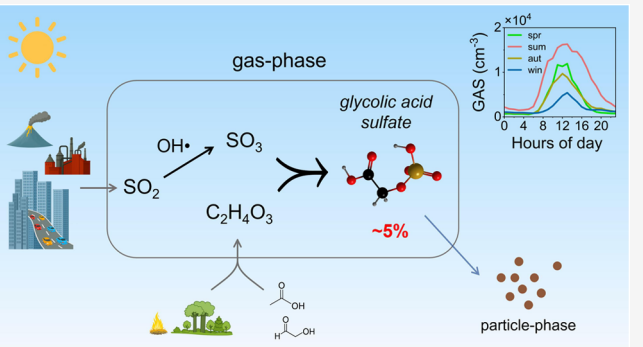

KEYWORDS: *organosulfates, glycolic acid sulfate, extremely low-volatility compounds, gas-phase, sulfur trioxide*

1. INTRODUCTION

Secondary organic aerosols (SOAs) are known to influence climate,[1,2] air quality,[3,4] and human health.[5] Organosulfates (OSs), which form through organic-sulfur interactions, are a significant class of compounds within SOAs.[6−9] Contributing 5−30% of organic matter in atmospheric particles, OSs have become a focal point in atmospheric chemistry research.[10−14] Their prevalence has been elucidated through extensive chamber[6−8,15,16] and field studies,[17−20] establishing OSs as key markers and tracers for SOA formation and aging processes.[10,14,21−23] Importantly, the high amphiphilic property of OSs allows them to lower the surface tension of atmospheric particles,[16,24,25] which in turn affects the physicochemical properties of aerosols, including hygroscopicity,[24,26] acidity,[25,27] and optical characteristics.[28]

Glycolic acid sulfate (GAS, $C_2H_4O_6S$), one of the simplest OSs containing both carboxyl and sulfate groups, is widely detected in ambient aerosols. Across various environmental conditions, GAS typically constitutes 5−20% of total detected organosulfates in ambient aerosol samples.[13,29,30] Notably, peak concentrations of 155.5 ng m^{-3} in Xi'an, China[31] and 149.3 ng m^{-3} in Tianjin, China[32] highlight potential extreme accumulations. Currently, GAS, like other OSs, is considered to form primarily in the aerosol phase through several key mechanisms: (1) heterogeneous reactions of gaseous organic precursors on acidic sulfate aerosols;[15,33] (2) recently proposed pathways involving sulfur trioxide (SO_3) acting as an electrophile or sulfuric acid (SA) as a nucleophile in reactions with oxygenated organic compounds;[34] and (3) potential formation through heterogeneous reactions between sulfur dioxide (SO_2) and unsaturated organic compounds.[18,35]

Recent studies have hinted at the intriguing possibility of GAS existing in the gas phase, challenging the long-held assumption that organosulfates are confined exclusively to the condensed phase. Ehn et al.[36] first proposed the possibility of gas-phase GAS based on measurements of air ions using an atmospheric pressure interface time-of-flight mass spectrometer (APi-TOF). Subsequent studies[34,37,38] using filter inlet for gases and aerosols coupled with iodide chemical ionization

Received: June 11, 2025
Revised: June 19, 2025
Accepted: June 23, 2025
Published: July 8, 2025

https://doi.org/10.1021/acs.est.5c07888
Environ. Sci. Technol. 2025, 59, 16556−16566

mass spectrometry (FIGAERO-I-CIMS) detected signals consistent with gas-phase GAS, suggesting that a non-negligible fraction might exist in the gas phase. These preliminary findings carry profound implications for atmospheric chemistry, particularly when considering potential analogies to gas-phase sulfuric acid—a critical precursor in new particle formation (NPF). Theoretical studies have already begun exploring potential implications, such as interactions between gas-phase GAS and Criegee intermediates[39] or its role in nucleation mechanisms involving sulfuric acid and dimethylamine.[39,40] Nevertheless, it is crucial to emphasize that the sources, formation mechanisms, and even the very existence of gas-phase organosulfates, including GAS, remain largely unconfirmed.

In this study, we present reliable measurements of gaseous GAS in the atmosphere using APi-TOF with nitrate ions as reagents (nitrate-APi-TOF). The measurements were conducted over four seasons in East China, a densely populated region that continues to face air pollution challenges despite improvements in air quality. We also employed FIGAERO-I-CIMS to investigate GAS gas-particle partitioning, providing evidence for its gas-phase existence and formation. By examining the relationships between all observed tracers and GAS, we proposed a mechanism for the gas-phase formation of GAS and estimated the rate of this reaction based on in situ observations.

2. METHODS

2.1. Site Description. Field campaigns were conducted at the Station for Observing Regional Processes of the Earth System (SORPES) (118° 57′ E, 32° 07′ N) on the Xianlin campus of Nanjing University, eastern China. The station captures urban-scale emission activity[41] and is frequently impacted by polluted air masses from the North China Plain and the Yangtze River Delta urban agglomeration.[42,43] Detailed descriptions of the station can be found in previous studies.[42,44,45] In this work, one campaign for FIGAERO-I-CIMS was conducted in August 2021, and other campaigns for nitrate-APi-TOF were conducted in August 2022 (summer), from September to November 2022 (autumn), from December 2022 to February 2023 (winter), and from April to May 2023 (spring).

2.2. Detection of Gaseous GAS by Mass Spectrometry Techniques. Nitrate-APi-TOF (Aerodyne Research Inc.) was deployed to measure gas-phase GAS (Figures S1a and S2) and glycolic acid (GA, Figures S2 and S3). The working principle[46] and sampling configuration[47−49] of nitrate-APi-TOF have been described in previous studies. GAS was quantified using the calibration factor for sulfuric acid, under the assumption of a similar ionization efficiency.[50] The applied calibration factors were determined to be 3.9×10^9 cm^{-3} $ncps^{-1}$ (spring) and 3.2×10^9 cm^{-3} $ncps^{-1}$ (other seasons) through in situ-generated sulfuric acid. GA was quantified using the calibration factor for HONO, also assuming a comparable ionization efficiency (Figure S4). The applied calibration factor was determined to be 1.2×10^{13} cm^{-3} $ncps^{-1}$ through parallel HONO measurements (Figure S5), which aligns with values previously reported for small organic acids.[51] In addition, the detection limit of GAS was determined as the sum of the mean and three times the standard deviation during the zeroing period ($\bar{x} + 3\sigma$), with details provided in Text S1 and Figure S6.

FIGAERO-I-CIMS (Aerodyne Research Inc.) was employed to simultaneously measure gas- and particle-phase GAS (Figure S1b). The operational principles have been extensively described in previous studies.[52] In our measurements, each sampling cycle included particle collection, followed by thermal desorption under a controlled temperature program (Figure S7). Detailed descriptions of the FIGAERO operation and other measurements are provided in Text S2 and S3, respectively.

Due to the high propensity of gas-phase organosulfates to undergo wall losses during sampling, we recommend nitrate-APi-TOF as the preferred detection method. This approach aligns with established techniques for measuring gas-phase sulfuric acid, another low-volatility compound with similar sampling challenges. The instrument's high flow rates, large inlet diameters, and laminar flow configuration between sheath and sample flows effectively minimize wall losses.[53] Accordingly, in this study, nitrate-APi-TOF was used to measure gas-phase GAS concentrations and analyze their formation mechanisms, while FIGAERO-I-CIMS was employed to examine their gas-particle partitioning behavior.

2.3. P_{sat}−T_{max} Linear Relationship of the FIGAERO Filter. For a certain compound, the temperature of the maximum desorption signal (T_{max}) derived from FIGAERO thermal profiles corresponds to its volatility property.[52] Based on a series of substances with known saturation vapor pressure P_{sat} (Pa) at 298 K, a linear relationship between P_{sat} and T_{max} was established through FIGAERO experiments,[52,54] in the following form

$$\log_{10}(P_{sat}) = aT_{max} + b, \text{ with } T_{max} \text{ in } (^\circ C) \quad \text{(E1)}$$

where a and b are fitted parameters. Further, P_{sat} can be converted to saturation mass concentration (C^*) using the ideal gas law,[55,56] leading to the following relationship between C^* and T_{max}

$$C^*(\mu g\ m^{-3}) = 10^6 \frac{(10^{aT_{max}+b})M_w}{RT} \quad \text{(E2)}$$

where M_w is the molar mass of the compound (g mol^{-1}), R is the gas constant (8.314 J mol^{-1} K^{-1}), and T is 298 K.

2.4. Theoretical Gas-Particle Partitioning of GAS. To compare the observed gas-particle partitioning of GAS (eq E3) with the equilibrium level, we applied the gas-particle equilibrium theory first described by Pankow.[57] Instead of the commonly used particle-phase fraction as the partitioning coefficient,[58−60] we used the gas-phase fraction (F_g) to illustrate the notable ratio of GAS in the gas phase (eq E4).

$$F_g = \frac{\text{gas}}{\text{gas} + \text{particle}} \quad \text{(E3)}$$

$$F_g = 1 - \left(1 + \frac{\frac{M10^6\gamma P}{760RT}}{C_{OA}}\right)^{-1} \quad \text{(E4)}$$

where T (K) is the environmental temperature, and γ is the activity coefficient, which is semiempirically predicted by a polynomial equation.[61] M (g mol^{-1}) is the molar mass of the glycolic acid sulfate (~156), and R (8.2×10^{-5} m^3 atm K^{-1} mol^{-1}) is the gas constant. C_{OA} ($\mu g\ m^{-3}$) is the organic aerosol mass concentration, which was measured by ACSM (described in the Supporting Information). P (torr) is the saturated vapor pressure of the compound, which is calculated based on the linear P_{sat}−T_{max} relationship of FIGAERO. Furthermore, the Clausius−Clapeyron equation was used to obtain P (torr) at

https://doi.org/10.1021/acs.est.5c07888
Environ. Sci. Technol. 2025, 59, 16556−16566

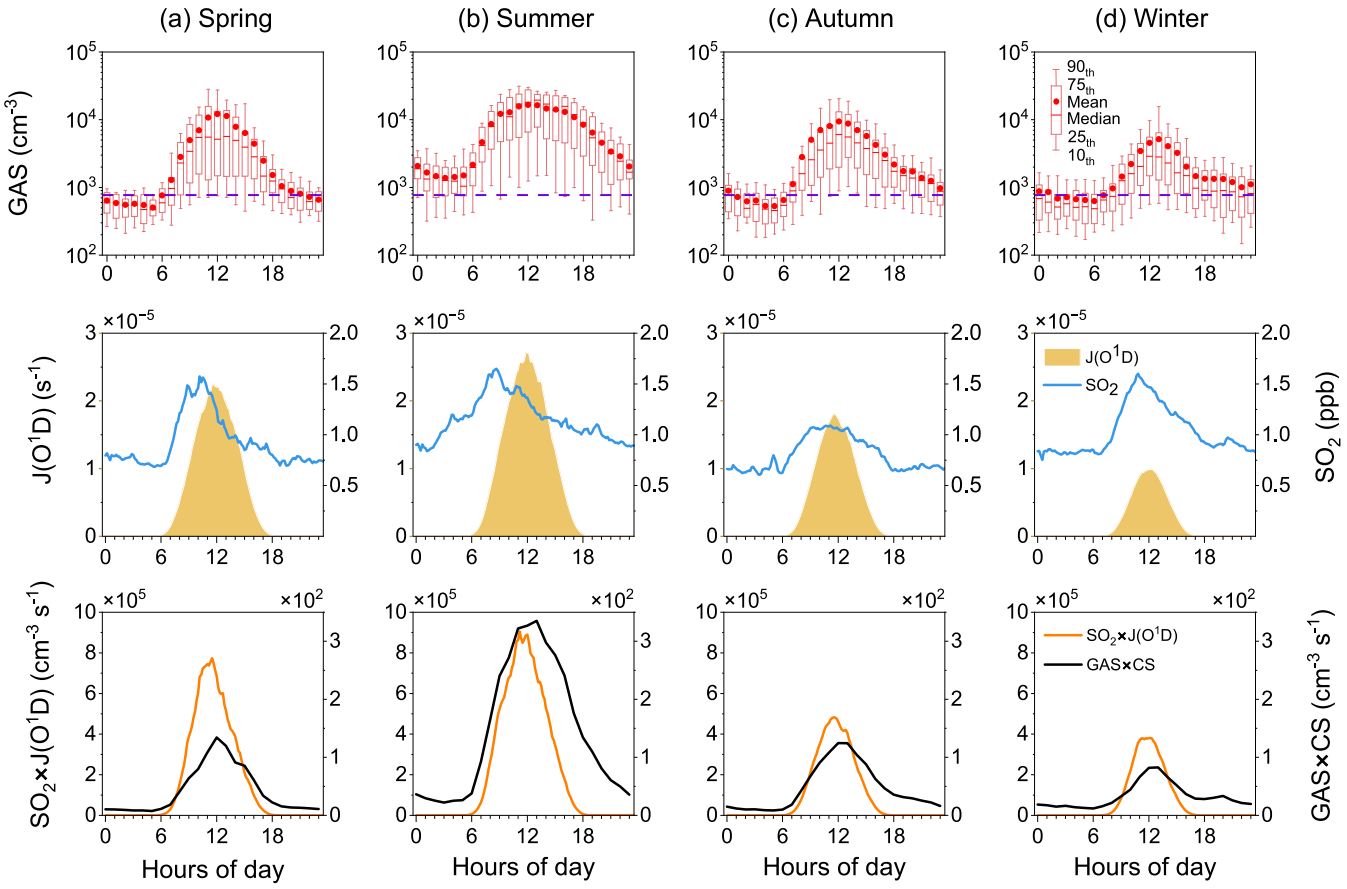

Figure 1. Diurnal variations of J(O^{1}D), SO_2, GAS, SO_2 × J(O^{1}D), and GAS × CS in (a) spring, (b) summer, (c) autumn, and (d) winter. The purple dashed lines in panels (a–d) represent the detection limit of GAS (8×10^2 cm^{-3}). The levels of J(O^{1}D), SO_2, SO_2 × J(O^{1}D), and GAS × CS are displayed as their mean concentrations.

different temperatures. Additionally, the calculations of the vaporization enthalpy (ΔH_{vap}) are based on equations refined from the Abraham model, with details provided by Churchill et al.[62]

2.5. SO_3 Simulation. SO_3 is a critical intermediate in atmospheric sulfur chemistry, primarily formed through the gas-phase oxidation of SO_2 and rapidly converted to sulfuric acid by abundant atmospheric water vapor.[63] With an extremely short atmospheric lifetime, SO_3 chemistry is governed by local processes, making it ideal for observation-constrained simulations. We utilized the Master Chemical Mechanism (MCM version 3.3.1, https://mcm.york.ac.uk/MCM/, last access: 25 November 2024) to calculate SO_3 concentrations across four seasons, with measured SO_2 concentrations and estimated hydroxyl radicals (OH) as key inputs. The model considered the oxidation of SO_2 by OH radicals as the main production pathway and hydrolysis with water vapor as the dominant loss mechanism for SO_3. Model validation was performed by comparing the derived and observed SA concentrations, showing strong agreement (Figure S8). SA was produced through SO_3 hydrolysis with water vapor, while its removal was governed by three major loss processes: condensation sink, dry deposition, and molecular clustering, following Yang et al.[64] The OH concentrations used in the model were calculated as a function of measured ozone photolysis frequencies J(O^{1}D), as detailed in Figure S9.

2.6. Calculation of the Reaction Rate Constant for SO_3 and GA. The proposed pathway for GAS formation is as follows

$$SO_3 + C_2H_4O_3\ (GA) \rightarrow C_2H_4O_6S\ (GAS) \quad (R1)$$

As an ELVOC, the condensation of gas-phase GAS onto particles can be considered effectively irreversible. Therefore, we assume that its atmospheric behavior is similar to that of gas-phase sulfuric acid and that its temporal evolution is mainly governed by local processes. The time-dependent concentration of GAS can thus be expressed by the following equation

$$\frac{d[GAS]}{dt} = k[SO_3][GA] - [GAS] \times CS \quad (E5)$$

where the first term on the right-hand side represents the production rate of gas-phase GAS, while the second term accounts for its loss due to condensation onto particles. [SO_3], [GA], and [GAS] are the concentrations of SO_3, GA, and GAS, respectively. CS denotes the condensation sink (s^{-1}).

Under the assumption that GAS reaches a quasi-steady state in the atmosphere, the production rate equals the loss rate. Consequently, the reaction rate constant k can be calculated as follows

$$k = \frac{[GAS] \times CS}{[SO_3][GA]} \quad (E6)$$

2.7. Contribution Assessment of Gas-Phase GAS to Particulate GAS. We adopted a simplified method proposed

https://doi.org/10.1021/acs.est.5c07888
Environ. Sci. Technol. 2025, 59, 16556−16566

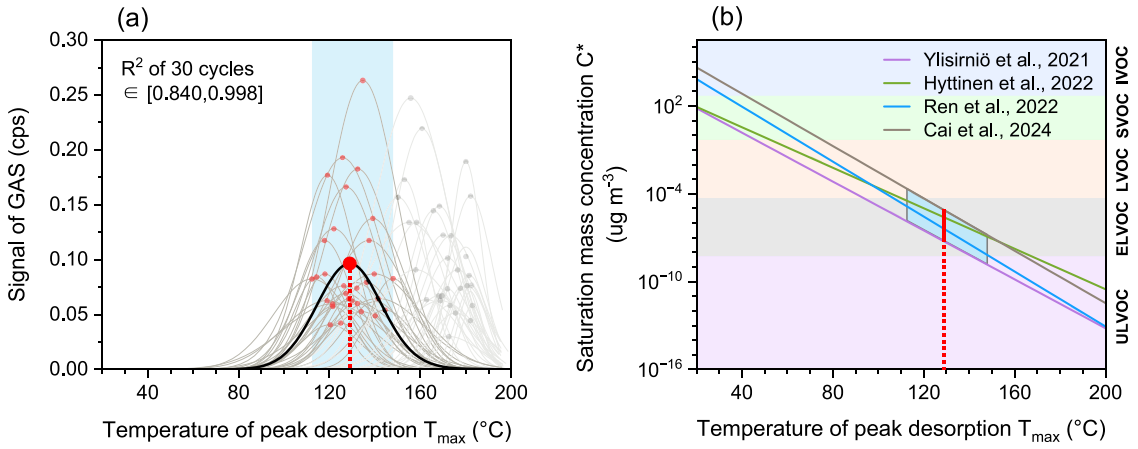

Figure 2. Volatility determination of GAS based on FIGAERO-I-CIMS measurements. (a) Gaussian bimodal fit of 30 thermal desorption processes for GAS, with R^2 values ranging from 0.840 to 0.998. The gray fitted lines indicate the first peaks of the 30 cycles, while the light gray lines represent the second peaks, with dots corresponding to T_{max} values. The black line represents the average fit (T_{max} = 128.9 °C; red dot and dashed line), with the blue shading indicating the T_{max} range (112.3−148.0 °C) of the included peaks. (b) Four previously reported calibration measurements with T_{max} plotted against the saturation mass concentration C^* based on atomizer methods, color-filled based on the VBS proposed by Tröstl et al.[75] The red line and blue shading correspond to those in panel (a), respectively.

by Wang et al.[65] to estimate the amount of gas-phase GAS that may condense onto particles during their typical atmospheric lifetime. Specifically, we evaluated the cumulative condensation flux of gas-phase GAS over a 5-day period, representing the average residence time of particles in this region.[65] The condensation amount was calculated by integrating the product of the gas-phase GAS concentration and CS during stable planetary boundary layer periods (11:00−15:00 daily) as follows

$$\mathrm{GAS_{cond}} = \int (\mathrm{GAS} \times \mathrm{CS})\mathrm{d}t \tag{E7}$$

The resulting cumulative GAS condensation flux over 5 days was then compared to reported particulate GAS concentrations (Figure S10), as our FIGAERO measurements were not specifically calibrated for GAS. This comparison allowed us to estimate the relative contribution of gas-phase condensation to the particulate GAS budget under typical atmospheric conditions.

3. RESULTS

3.1. Seasonal and Diurnal Behavior of GAS. As shown in Figure 1, GAS exhibited distinct diurnal and seasonal patterns with concentrations peaking around midday across all seasons. The highest levels were observed in summer, reaching a maximum average of 4.6 × 10^4 cm^{-3}, followed by progressively lower concentrations in spring (3.8 × 10^3 cm^{-3}), autumn (3.6 × 10^3 cm^{-3}), and winter (2.1 × 10^3 cm^{-3}). This pronounced temporal pattern suggests a photochemically driven formation, supported by several lines of evidence: the diurnal variation of GAS closely tracks those of the ozone photolysis rate [$J(O^1D)$] and its product with SO_2 ($SO_2 \times J(O^1D)$) (Figure 1); a strong positive correlation (r = 0.54−0.70) between GAS and sulfuric acid was observed across all seasons (Figure S11), suggesting shared photochemical generation pathways; and the inverse relationship between GAS and $PM_{2.5}$ (Figure S12) implies that particulate matter functions primarily as a sink rather than a source. Given that GAS is characterized as an extremely low-volatility compound (as demonstrated in subsequent sections), which is highly susceptible to condensation loss, we applied the steady-state assumption analogous to sulfuric acid, where the production rate equals the loss rate. Under this framework, the product of the GAS concentration and condensation sink (GAS × CS) averages above 1 × 10^2 cm^{-3} s^{-1} during midday (Figure 1), with peak values reaching 1.2 × 10^3 cm^{-3} s^{-1}, representing both a significant gas-phase production and a considerable contribution to aerosol organosulfate loading.

3.2. Volatility Characterization of GAS Using FIGAERO Thermal Desorption. The volatility of GAS was evaluated by using thermal desorption profiles obtained from FIGAERO field measurements. This method relies on the established relationship between T_{max} and the compound volatility, typically expressed as C^*.[52,54,66] We analyzed 30 thermal desorption profiles where GAS signals exceeded 0.01 cps, with each profile consistently exhibiting a characteristic double-peak structure (Figure S13). The first peak was attributed to GAS, while the second peak likely resulted from the decomposition of higher-molecular-weight compounds.[54] A double-peak Gaussian fitting was applied to each thermal desorption profile to determine the T_{max} for GAS. The results showed T_{max} values ranging from 112.3 to 148.0 °C, with an average of 128.9 °C (Figure 2a). This variability in ambient measurements can be attributed to matrix effects, where diverse particle components interact during thermal desorption, reflecting the complexity of real atmospheric conditions.[54,67]

To interpret these T_{max} values in terms of volatility, we employed four C^*-T_{max} relationships derived from atomizer methods in previous studies[56,68−70] (Figure 2b). Notably, as Ylisirniö et al.[68] proposed, these atomizer methods can more accurately capture the evaporation of chemical constituents from ambient aerosol particles compared to the syringe methods used in earlier studies.[52,54,58,71] The background shown in Figure 2b illustrates the volatility ranges based on established classification schemes: ultralow-volatility organic compounds (ULVOCs; $C^* < 10^{-8.5}$ $\mu g\ m^{-3}$), extremely low-volatility organic compounds (ELVOCs; $10^{-8.5} < C^* < 10^{-4.5}$ $\mu g\ m^{-3}$), low-volatility organic compounds (LVOCs, $10^{-4.5} < C^* < 10^{-0.5}$ $\mu g\ m^{-3}$), semivolatile organic compounds (SVOCs; $10^{-0.5} < C^* < 10^{2.5}$ $\mu g\ m^{-3}$), intermediate-volatility

https://doi.org/10.1021/acs.est.5c07888
Environ. Sci. Technol. 2025, 59, 16556−16566

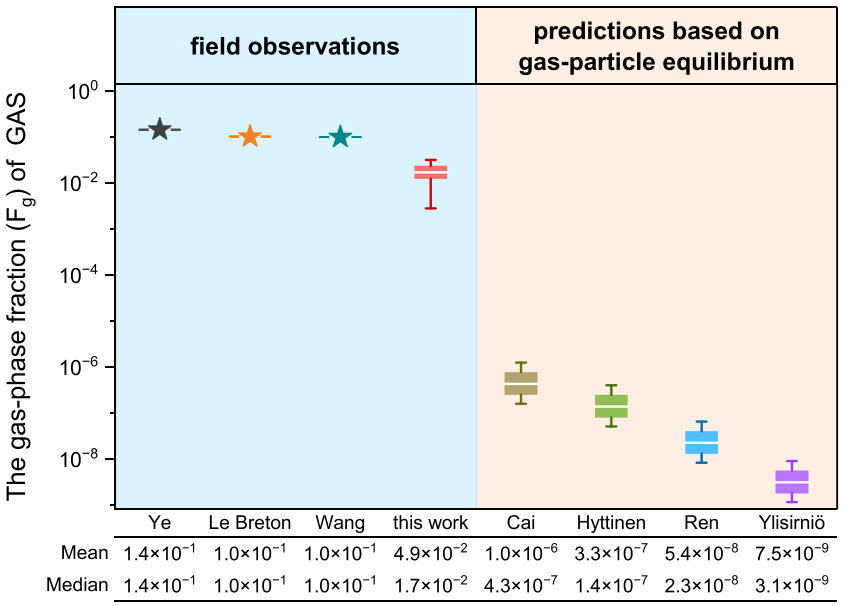

Figure 3. Evidence of GAS gas-phase formation. The three pentagrams represent values from FIGAERO measurements of Ye et al.,[37] Le Breton et al.[38] and Wang et al.,[34] respectively, while the red box indicates results from our observations. The four boxes on the right display the gas fractions of GAS at gas-particle equilibrium. In the calculations, the saturated vapor pressure is derived from the four $P_{sat}-T_{max}$ relationships shown in Figure 2b, using T_{max} at 128.9 °C (Figure 2a).

organic compounds (IVOCs; $10^{2.5} < C^* < 10^{6.5}$ $\mu g\ m^{-3}$), and volatile organic compounds (VOCs; $C^* > 10^{6.5}$ $\mu g\ m^{-3}$).[72−74]

Based on the average T_{max} of 128.9 °C, GAS is classified as an ELVOC according to these relationships. This classification suggests that GAS should predominantly exist in the particle phase upon gas-particle partition. To further investigate this implication, we compared the observed gas-phase fractions (F_gs) of GAS with those predicted under gas-particle equilibrium conditions. Our field measurements showed an average gas-phase fraction of GAS around 5%, which is consistent with previous studies reporting GAS F_gs of 10.0% in Hong Kong,[34] 14.5% in Guangzhou,[37] and 10.2% in Beijing.[38] In contrast, the calculated equilibrium F_gs for GAS, derived using Pankow equations and vapor pressures from the $P_{sat}-T_{max}$ relationships, ranged from 3.9×10^{-9} to 5.2×10^{-7} (Figure 3). The observed gas-phase proportion of GAS in the real atmosphere significantly exceeds these equilibrium estimates by 5−7 orders of magnitude. This enormous discrepancy yields two critical conclusions. First, gas-phase GAS cannot originate from aerosol-phase GAS evaporation as observed concentrations vastly exceed what particle-to-gas partitioning could explain. Second, unexpectedly high gas-phase GAS concentrations necessitate significant gas-phase formation pathways. Overall, as an ELVOC, once formed in the gas phase, GAS irreversibly condenses onto aerosol particles, while GAS in the aerosol phase is unlikely to revolatilize back into the gas phase.

3.3. Potential Gas-Phase Reaction of SO_3 with GA to Form GAS. Further, we conducted a comprehensive correlation analysis between GAS and various atmospheric tracers to elucidate potential formation pathways (Figure S11). Notably, we found significant correlations between GAS and SO_3, GA, and the product of SO_3 and GA concentrations (Figures 4 and S11). This observation led us to hypothesize a potential gas-phase formation mechanism for GAS involving SO_3 and GA.

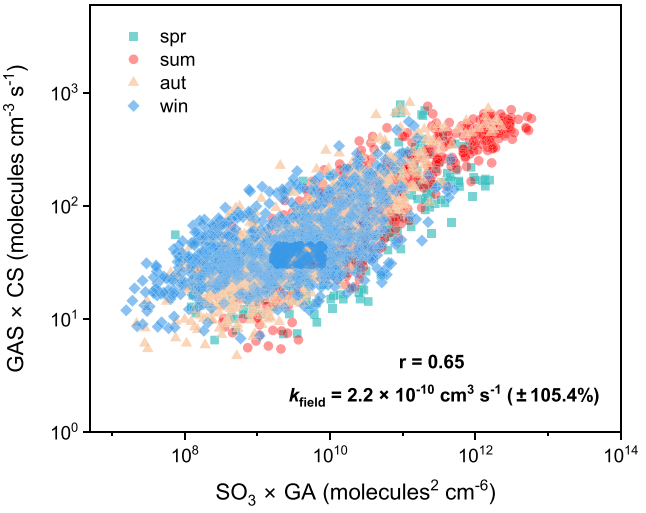

Figure 4. Gas-phase formation of GAS via the reaction between SO_3 and GA. The product of SO_3 and GA shows a linear correlation of 0.65 with the production rate of GAS (GAS × CS, $cm^{-3}\ s^{-1}$) across all four seasons. Under steady-state assumptions, the field-based reaction rate constant (k_{field}) is calculated as 2.2×10^{-10} $cm^3\ s^{-1}$ (limited to cases with GAS > 1000 cm^{-3}). Scatter points are colored differently for each season.

The proposed mechanism exhibits the following chemical plausibility: GA can provide the carbon skeleton and carboxyl group for GAS, while SO_3 contributes the sulfate functional group. This hypothesis is supported by recent quantum chemical calculations, which have shown the feasibility of such reactions in the gas phase.[40,76] In the esterification reaction, the hydroxyl oxygen atom in GA could react with the sulfur atom in SO_3 to form GAS, accompanied by the concurrent proton transfer from GA to SO_3, in which the catalyst H_2O or SA could make the reaction barrierless. Additionally, it is worth noting that the product GAS, with a more negative Gibbs free energy of formation, is thermody-

https://doi.org/10.1021/acs.est.5c07888
Environ. Sci. Technol. 2025, 59, 16556−16566

namically more stable than glycolic acid sulfuric anhydride—another possible product of the SO_3 and GA reaction—whose atmospheric concentration was calculated to be negligible.[40]

As an ELVOC, gas-phase GAS likely maintains a quasi-steady state with balanced source and sink rates. By combining the gas-phase GAS concentration with its condensation sink, MCM-derived SO_3 concentration, and observed GA levels, we estimated a field-based reaction rate constant of 2.2×10^{-10} $cm^3\ s^{-1}$ (eq E6). Notably, our estimated reaction rate constant approaches the collision limit, comparable to reported rates for SO_3-acid reactions,[77] substantially higher than the SO_3-water rate constant and slightly exceeding that of SO_3 with water dimers.[63] This high reactivity explains Friedman et al.'s[78] observation of organics competing with water for SO_3 in laboratory settings. However, in the ambient atmosphere, water concentrations (typically 10^{18}–10^{20} molecules cm^{-3}) vastly exceed those of glycolic acid and similar organic compounds (typically 10^{8}–10^{10} molecules cm^{-3}). Consequently, water dominates as the primary SO_3 sink under typical conditions, yielding sulfuric acid, except in extremely dry, organic-rich environments. Although competition with water for SO_3 is generally limited, this alternative pathway can still serve as a significant source of gas-phase organosulfates, becoming especially pronounced in environments, such as volcanic plumes, wildfire smoke, or certain industrial emissions.

There are uncertainties in our rate coefficient estimation. The error in simulated SO_3 from MCM can be derived from the SA results. Considering the 50% uncertainty in SA observations[79] and the 63.3% uncertainty introduced by model calculations, the final uncertainty of SO_3 is determined to be 80.7% (calculated from $\sqrt{(50\%)^2 + (63.3\%)^2}$). As noted in a recent study,[51] the calibration coefficient for dicarboxylic acids exhibits an uncertainty between 30% and 66%. In this study, the uncertainty of GA concentrations is assumed to be the mean value of 45.8%. Additionally, the uncertainty of GAS concentrations is predominantly influenced by the calibration processes, with a systematic uncertainty of 50%. Taking these factors into account, the total uncertainty of the reaction rate constant can be determined accordingly 105.4% (calculated from $\sqrt{(80.7\%)^2 + (45.8\%)^2 + (50\%)^2}$). Despite these uncertainties in rate constant quantification, the observed relationship between SO_3, GA, and GAS formation remains clear. Future studies are needed to constrain these uncertainties and further investigate the proposed formation pathway.

3.4. Atmospheric Implications. This study provides the first systematic field evidence for the consistent presence of a gas-phase organosulfate, GAS, in the atmosphere. We identified GAS as an ELVOC and discovered that its gas-phase fraction substantially exceeded predictions based on gas-particle equilibrium, underscoring the necessity of its gas-phase formation pathway.

The gas-phase formation of GAS has significant atmospheric implications. First, it offers an alternative perspective to the traditional understanding that organosulfates primarily form in the condensed phase. Comparing the cumulative condensation flux of gas-phase GAS over typical atmospheric particle lifetimes with reported particulate GAS concentrations, we estimate that gas-phase condensation contributes approximately 15.6% to the particulate GAS burden (Figure S10). This highlights the importance of gas-phase processes in the overall organosulfate budget. Second, this represents a novel source class of ELVOCs, expanding our understanding beyond previously established formation pathways. ELVOCs are known to participate in new particle formation, which typically supplies seed aerosols for secondary organic aerosol accumulation.

Our analysis further identified the reaction between SO_3 and GA as a potential mechanism for gas-phase GAS formation. The near-collision-limit reaction rate constant, derived from field data, suggests that SO_3 could play a far more significant role in gas-phase organic chemistry than previously recognized. This finding aligns with recent studies exploring SO_3's high reactivity with various organic compounds in the gas phase, including carboxylic acids[77] and alcohols.[76] Collectively, these insights necessitate a re-evaluation of SO_3's role in atmospheric chemistry, particularly regarding organosulfate formation and low-volatility organic compounds.

To extend our findings, we incorporated observational data from Suzhou, Shanghai, and Hong Kong in China (Figure S14), demonstrating the widespread presence of gas-phase GAS. However, our study is limited by the identification of only one gas-phase-formed organosulfate. Further research is needed to explore the potential presence of other gas-phase organosulfates across various environments and to evaluate the universality of their formation pathways and broader atmospheric implications. Additionally, further investigation is required to elucidate the detailed mechanisms underlying the gas-phase formation of organosulfates, with key areas of focus including the kinetic parameters of SO_3 reactions with relevant organic precursors and the potential existence of other, yet-unknown formation mechanisms.

■ ASSOCIATED CONTENT

Supporting Information

The Supporting Information is available free of charge at https://pubs.acs.org/doi/10.1021/acs.est.5c07888.

Supporting description of the detection limit (Text S1); supporting description of FIGAERO-I-CIMS (Text S2); supporting measurements (Text S3); high-resolution peak fit of the peak $C_2H_3O_6S^-$ (Figure S1); time series of GAS, GA, and SO_3 (Figure S2); high-resolution peak fit of the peak $C_2H_3O_3^-$ (Figure S3); calculated binding energies of $C_2H_4O_3$ and HONO (Figure S4); calibration factor derived from HONO data (Figure S5); determination of the GAS detection limit (Figure S6); FIGAREO sampling mode (Figure S7); SA concentrations from MCM simulations versus observations (Figure S8); observed OH radical versus $J(O^1D)$ (Figure S9); contribution of gaseous GAS to particulate GAS (Figure S10); correlation between GAS and various atmospheric tracers (Figure S11); gaseous GAS versus $PM_{2.5}$ (Figure S12); GAS desorption thermograms in the FIGAERO inlet (Figure S13); and concentrations of gaseous GAS at other sites (Figure S14) (PDF)

■ AUTHOR INFORMATION

Corresponding Authors

Yuliang Liu − *Joint International Research Laboratory of Atmospheric and Earth System Research, School of Atmospheric Sciences, Nanjing University, Nanjing 210023, China; National Observation and Research Station for Atmospheric Processes and Environmental Change in Yangtze*

https://doi.org/10.1021/acs.est.5c07888
Environ. Sci. Technol. 2025, 59, 16556−16566

River Delta, Nanjing 210023, China; orcid.org/0000-0002-0028-9102; Email: liuyuliang@nju.edu.cn

Wei Nie − *Joint International Research Laboratory of Atmospheric and Earth System Research, School of Atmospheric Sciences, Nanjing University, Nanjing 210023, China; National Observation and Research Station for Atmospheric Processes and Environmental Change in Yangtze River Delta, Nanjing 210023, China;* orcid.org/0000-0002-6048-0515; Email: niewei@nju.edu.cn

Authors

Haowei Sun − *Joint International Research Laboratory of Atmospheric and Earth System Research, School of Atmospheric Sciences, Nanjing University, Nanjing 210023, China; National Observation and Research Station for Atmospheric Processes and Environmental Change in Yangtze River Delta, Nanjing 210023, China*

Yuanyuan Li − *Joint International Research Laboratory of Atmospheric and Earth System Research, School of Atmospheric Sciences, Nanjing University, Nanjing 210023, China; National Observation and Research Station for Atmospheric Processes and Environmental Change in Yangtze River Delta, Nanjing 210023, China*

Dafeng Ge − *Joint International Research Laboratory of Atmospheric and Earth System Research, School of Atmospheric Sciences, Nanjing University, Nanjing 210023, China; National Observation and Research Station for Atmospheric Processes and Environmental Change in Yangtze River Delta, Nanjing 210023, China*

Tao Xu − *Joint International Research Laboratory of Atmospheric and Earth System Research, School of Atmospheric Sciences, Nanjing University, Nanjing 210023, China; National Observation and Research Station for Atmospheric Processes and Environmental Change in Yangtze River Delta, Nanjing 210023, China*

Junchao Yin − *Joint International Research Laboratory of Atmospheric and Earth System Research, School of Atmospheric Sciences, Nanjing University, Nanjing 210023, China; National Observation and Research Station for Atmospheric Processes and Environmental Change in Yangtze River Delta, Nanjing 210023, China*

Chong Liu − *Hubei Key Laboratory of Pollution Damage Assessment and Environmental Health Risk Prevention and Control, Hubei Provincial Academy of Eco-Environmental Sciences, Wuhan 430072, China*

Zihao Fu − *State Key Laboratory of Regional Environment and Sustainability, International Joint Laboratory for Regional Pollution Control, Ministry of Education (IJRC), College of Environmental Sciences and Engineering, Peking University, Beijing 100871, China*

Ximeng Qi − *Nanjing-Helsinki Institute in Atmospheric and Earth System Sciences, Nanjing University, Nanjing 210023, China; National Observation and Research Station for Atmospheric Processes and Environmental Change in Yangtze River Delta, Nanjing 210023, China;* orcid.org/0000-0002-7840-8239

Tengyu Liu − *Joint International Research Laboratory of Atmospheric and Earth System Research, School of Atmospheric Sciences, Nanjing University, Nanjing 210023, China; National Observation and Research Station for Atmospheric Processes and Environmental Change in Yangtze River Delta, Nanjing 210023, China;* orcid.org/0000-0002-3137-5898

Qiaozhi Zha − *Joint International Research Laboratory of Atmospheric and Earth System Research, School of Atmospheric Sciences, Nanjing University, Nanjing 210023, China; National Observation and Research Station for Atmospheric Processes and Environmental Change in Yangtze River Delta, Nanjing 210023, China*

Chao Yan − *Nanjing-Helsinki Institute in Atmospheric and Earth System Sciences, Nanjing University, Nanjing 210023, China; National Observation and Research Station for Atmospheric Processes and Environmental Change in Yangtze River Delta, Nanjing 210023, China*

Zhe Wang − *Division of Environment and Sustainability, The Hong Kong University of Science and Technology, Kowloon, Hong Kong SAR 999077, China;* orcid.org/0000-0002-5627-6562

Xuguang Chi − *Joint International Research Laboratory of Atmospheric and Earth System Research, School of Atmospheric Sciences, Nanjing University, Nanjing 210023, China; National Observation and Research Station for Atmospheric Processes and Environmental Change in Yangtze River Delta, Nanjing 210023, China*

Aijun Ding − *Joint International Research Laboratory of Atmospheric and Earth System Research, School of Atmospheric Sciences, Nanjing University, Nanjing 210023, China; National Observation and Research Station for Atmospheric Processes and Environmental Change in Yangtze River Delta, Nanjing 210023, China; Nanjing-Helsinki Institute in Atmospheric and Earth System Sciences, Nanjing University, Nanjing 210023, China;* orcid.org/0000-0003-4481-5386

Complete contact information is available at: https://pubs.acs.org/10.1021/acs.est.5c07888

Notes

The authors declare no competing financial interest.

■ ACKNOWLEDGMENTS

We thank colleagues and students at the School of Atmospheric Sciences at Nanjing University for their contributions to the maintenance of the measurements. We thank the tofTools team for providing tools for mass spectrometry analysis. This work was supported by the National Key Research and Development Program of China (2023YFC3706302), the National Natural Science Foundation of China (NSFC) (grants 42220104006, 42305119), the Jiangsu Province Outstanding Youth Fund (BK20240067), the Natural Science Foundation of Jiangsu Province (BK20230773), the Jiangsu Provincial Collaborative Innovation Center of Climate Change, and the Fundamental Research Funds for the Central Universities.

■ REFERENCES

(1) Shrivastava, M.; Cappa, C. D.; Fan, J.; Goldstein, A. H.; Guenther, A. B.; Jimenez, J. L.; Kuang, C.; Laskin, A.; Martin, S. T.; Ng, N. L.; Petaja, T.; Pierce, J. R.; Rasch, P. J.; Roldin, P.; Seinfeld, J. H.; Shilling, J.; Smith, J. N.; Thornton, J. A.; Volkamer, R.; Wang, J.; Worsnop, D. R.; Zaveri, R. A.; Zelenyuk, A.; Zhang, Q. Recent Advances in Understanding Secondary Organic Aerosol: Implications for Global Climate Forcing. *Rev. Geophys.* **2017**, *55* (2), 509−559.

(2) Tsigaridis, K.; Kanakidou, M. The Present and Future of Secondary Organic Aerosol Direct Forcing on Climate. *Curr. Clim. Change Rep.* **2018**, *4* (2), 84−98.

(3) Liu, L.; Kuang, Y.; Zhai, M.; Xue, B.; He, Y.; Tao, J.; Luo, B.; Xu, W.; Tao, J.; Yin, C.; Li, F.; Xu, H.; Deng, T.; Deng, X.; Tan, H.; Shao, M. Strong Light Scattering of Highly Oxygenated Organic Aerosols Impacts Significantly on Visibility Degradation. *Atmos. Chem. Phys.* **2022**, *22* (11), 7713−7726.
(4) Liang, C.-W.; Chang, C.-C.; Liang, J.-J. The Impacts of Air Quality and Secondary Organic Aerosols Formation on Traffic Accidents in Heavy Fog-Haze Weather. *Heliyon* **2023**, *9* (4), No. e14631.
(5) Offer, S.; Hartner, E.; Di Bucchianico, S.; Bisig, C.; Bauer, S.; Pantzke, J.; Zimmermann, E. J.; Cao, X.; Binder, S.; Kuhn, E.; Huber, A.; Jeong, S.; Käfer, U.; Martens, P.; Mesceriakovas, A.; Bendl, J.; Brejcha, R.; Buchholz, A.; Gat, D.; Hohaus, T.; Rastak, N.; Jakobi, G.; Kalberer, M.; Kanashova, T.; Hu, Y.; Ogris, C.; Marsico, A.; Theis, F.; Pardo, M.; Gröger, T.; Oeder, S.; Orasche, J.; Paul, A.; Ziehm, T.; Zhang, Z.-H.; Adam, T.; Sippula, O.; Sklorz, M.; Schnelle-Kreis, J.; Czech, H.; Kiendler-Scharr, A.; Rudich, Y.; Zimmermann, R. Effect of Atmospheric Aging on Soot Particle Toxicity in Lung Cell Models at the Air-Liquid Interface: Differential Toxicological Impacts of Biogenic and Anthropogenic Secondary Organic Aerosols (SOAs). *Environ. Health Perspect.* **2022**, *130* (2), No. 027003.
(6) Iinuma, Y.; Böge, O.; Kahnt, A.; Herrmann, H. Physical Chemistry of Aerosols. *Phys. Chem. Chem. Phys.* **2009**, *11* (36), 7985−7997.
(7) Surratt, J. D.; Kroll, J. H.; Kleindienst, T. E.; Edney, E. O.; Claeys, M.; Sorooshian, A.; Ng, N. L.; Offenberg, J. H.; Lewandowski, M.; Jaoui, M.; Flagan, R. C.; Seinfeld, J. H. Evidence for Organosulfates in Secondary Organic Aerosol. *Environ. Sci. Technol.* **2007**, *41* (2), 517−527.
(8) Surratt, J. D.; Gómez-González, Y.; Chan, A. W. H.; Vermeylen, R.; Shahgholi, M.; Kleindienst, T. E.; Edney, E. O.; Offenberg, J. H.; Lewandowski, M.; Jaoui, M.; Maenhaut, W.; Claeys, M.; Flagan, R. C.; Seinfeld, J. H. Organosulfate Formation in Biogenic Secondary Organic Aerosol. *J. Phys. Chem. A* **2008**, *112* (36), 8345−8378.
(9) Fu, Z.; Ma, F.; Liu, Y.; Yan, C.; Huang, D.; Chen, J.; Elm, J.; Li, Y.; Ding, A.; Pichelstorfer, L.; Xie, H.-B.; Nie, W.; Francisco, J. S.; Zhou, P. An Overlooked Oxidation Mechanism of Toluene: Computational Predictions and Experimental Validations. *Chem. Sci.* **2023**, *14* (45), 13050−13059.
(10) Froyd, K. D.; Murphy, S. M.; Murphy, D. M.; de Gouw, J. A.; Eddingsaas, N. C.; Wennberg, P. O. Contribution of Isoprene-Derived Organosulfates to Free Tropospheric Aerosol Mass. *Proc. Natl. Acad. Sci. U.S.A.* **2010**, *107* (50), 21360−21365.
(11) Tolocka, M. P.; Turpin, B. Contribution of Organosulfur Compounds to Organic Aerosol Mass. *Environ. Sci. Technol.* **2012**, *46* (15), 7978−7983.
(12) Shakya, K. M.; Peltier, R. E. Non-Sulfate Sulfur in Fine Aerosols across the United States: Insight for Organosulfate Prevalence. *Atmos. Environ.* **2015**, *100*, 159−166.
(13) Glasius, M.; Bering, M. S.; Yee, L. D.; de Sá, S. S.; Isaacman-VanWertz, G.; Wernis, R. A.; Barbosa, H. M. J.; Alexander, M. L.; Palm, B. B.; Hu, W.; Campuzano-Jost, P.; Day, D. A.; Jimenez, J. L.; Shrivastava, M.; Martin, S. T.; Goldstein, A. H. Organosulfates in Aerosols Downwind of an Urban Region in Central Amazon. *Environ. Sci.: Processes Impacts* **2018**, *20* (11), 1546−1558.
(14) Brüggemann, M.; Poulain, L.; Held, A.; Stelzer, T.; Zuth, C.; Richters, S.; Mutzel, A.; van Pinxteren, D.; Iinuma, Y.; Katkevica, S.; Rabe, R.; Herrmann, H.; Hoffmann, T. Real-Time Detection of Highly Oxidized Organosulfates and BSOA Marker Compounds during the F-Beach 2014 Field Study. *Atmos. Chem. Phys.* **2017**, *17* (2), 1453−1469.
(15) Galloway, M. M.; Chhabra, P. S.; Chan, A. W. H.; Surratt, J. D.; Flagan, R. C.; Seinfeld, J. H.; Keutsch, F. N. Glyoxal Uptake on Ammonium Sulphate Seed Aerosol: Reaction Products and Reversibility of Uptake under Dark and Irradiated Conditions. *Atmos. Chem. Phys.* **2009**, *9* (10), 3331−3345.
(16) Nozière, B.; Ekström, S.; Alsberg, T.; Holmström, S. Radical-Initiated Formation of Organosulfates and Surfactants in Atmospheric Aerosols. *Geophys. Res. Lett.* **2010**, *37* (5), No. L05806.
(17) Stone, E. A.; Yang, L.; Yu, L. E.; Rupakheti, M. Characterization of Organosulfates in Atmospheric Aerosols at Four Asian Locations. *Atmos. Environ.* **2012**, *47*, 323−329.
(18) Brüggemann, M.; Xu, R.; Tilgner, A.; Kwong, K. C.; Mutzel, A.; Poon, H. Y.; Otto, T.; Schaefer, T.; Poulain, L.; Chan, M. N.; Herrmann, H. Organosulfates in Ambient Aerosol: State of Knowledge and Future Research Directions on Formation, Abundance, Fate, and Importance. *Environ. Sci. Technol.* **2020**, *54* (7), 3767−3782.
(19) Cai, D.; Wang, X.; Chen, J.; Li, X. Molecular Characterization of Organosulfates in Highly Polluted Atmosphere Using Ultra-High-Resolution Mass Spectrometry. *J. Geophys. Res.: Atmos.* **2020**, *125* (8), No. e2019JD032253.
(20) Wang, Y.; Ma, Y.; Kuang, B.; Lin, P.; Liang, Y.; Huang, C.; Yu, J. Z. Abundance of Organosulfates Derived from Biogenic Volatile Organic Compounds: Seasonal and Spatial Contrasts at Four Sites in China. *Sci. Total Environ.* **2022**, *806*, No. 151275.
(21) Kristensen, K.; Glasius, M. Organosulfates and Oxidation Products from Biogenic Hydrocarbons in Fine Aerosols from a Forest in North West Europe during Spring. *Atmos. Environ.* **2011**, *45* (27), 4546−4556.
(22) Worton, D. R.; Goldstein, A. H.; Farmer, D. K.; Docherty, K. S.; Jimenez, J. L.; Gilman, J. B.; Kuster, W. C.; de Gouw, J.; Williams, B. J.; Kreisberg, N. M.; Hering, S. V.; Bench, G.; McKay, M.; Kristensen, K.; Glasius, M.; Surratt, J. D.; Seinfeld, J. H. Origins and Composition of Fine Atmospheric Carbonaceous Aerosol in the Sierra Nevada Mountains, California. *Atmos. Chem. Phys.* **2011**, *11* (19), 10219−10241.
(23) Zhang, H.; Worton, D. R.; Lewandowski, M.; Ortega, J.; Rubitschun, C. L.; Park, J.-H.; Kristensen, K.; Campuzano-Jost, P.; Day, D. A.; Jimenez, J. L.; Jaoui, M.; Offenberg, J. H.; Kleindienst, T. E.; Gilman, J.; Kuster, W. C.; de Gouw, J.; Park, C.; Schade, G. W.; Frossard, A. A.; Russell, L.; Kaser, L.; Jud, W.; Hansel, A.; Cappellin, L.; Karl, T.; Glasius, M.; Guenther, A.; Goldstein, A. H.; Seinfeld, J. H.; Gold, A.; Kamens, R. M.; Surratt, J. D. Organosulfates as Tracers for Secondary Organic Aerosol (SOA) Formation from 2-Methyl-3-Buten-2-Ol (MBO) in the Atmosphere. *Environ. Sci. Technol.* **2012**, *46* (17), 9437−9446.
(24) Hansen, A. M. K.; Hong, J.; Raatikainen, T.; Kristensen, K.; Ylisirniö, A.; Virtanen, A.; Petäjä, T.; Glasius, M.; Prisle, N. L. Hygroscopic Properties and Cloud Condensation Nuclei Activation of Limonene-Derived Organosulfates and Their Mixtures with Ammonium Sulfate. *Atmos. Chem. Phys.* **2015**, *15* (24), 14071−14089.
(25) Riva, M.; Chen, Y.; Zhang, Y.; Lei, Z.; Olson, N. E.; Boyer, H. C.; Narayan, S.; Yee, L. D.; Green, H. S.; Cui, T.; Zhang, Z.; Baumann, K.; Fort, M.; Edgerton, E.; Budisulistiorini, S. H.; Rose, C. A.; Ribeiro, I. O.; Oliveira, R. L. E.; dos Santos, E. O.; Machado, C. M. D.; Szopa, S.; Zhao, Y.; Alves, E. G.; de Sá, S. S.; Hu, W.; Knipping, E. M.; Shaw, S. L.; Duvoisin Junior, S.; de Souza, R. A. F.; Palm, B. B.; Jimenez, J.-L.; Glasius, M.; Goldstein, A. H.; Pye, H. O. T.; Gold, A.; Turpin, B. J.; Vizuete, W.; Martin, S. T.; Thornton, J. A.; Dutcher, C. S.; Ault, A. P.; Surratt, J. D. Increasing Isoprene Epoxydiol-to-Inorganic Sulfate Aerosol Ratio Results in Extensive Conversion of Inorganic Sulfate to Organosulfur Forms: Implications for Aerosol Physicochemical Properties. *Environ. Sci. Technol.* **2019**, *53* (15), 8682−8694.
(26) Estillore, A. D.; Hettiyadura, A. P. S.; Qin, Z.; Leckrone, E.; Wombacher, B.; Humphry, T.; Stone, E. A.; Grassian, V. H. Water Uptake and Hygroscopic Growth of Organosulfate Aerosol. *Environ. Sci. Technol.* **2016**, *50* (8), 4259−4268.
(27) Zhang, Y.; Chen, Y.; Lei, Z.; Olson, N. E.; Riva, M.; Koss, A. R.; Zhang, Z.; Gold, A.; Jayne, J. T.; Worsnop, D. R.; Onasch, T. B.; Kroll, J. H.; Turpin, B. J.; Ault, A. P.; Surratt, J. D. Joint Impacts of Acidity and Viscosity on the Formation of Secondary Organic Aerosol from Isoprene Epoxydiols (IEPOX) in Phase Separated Particles. *ACS Earth Space Chem.* **2019**, *3* (12), 2646−2658.
(28) Fleming, L. T.; Ali, N. N.; Blair, S. L.; Roveretto, M.; George, C.; Nizkorodov, S. A. Formation of Light-Absorbing Organosulfates during Evaporation of Secondary Organic Material Extracts in the

Presence of Sulfuric Acid. *ACS Earth Space Chem.* **2019**, *3* (6), 947−957.
(29) Rattanavaraha, W.; Chu, K.; Budisulistiorini, S. H.; Riva, M.; Lin, Y.-H.; Edgerton, E. S.; Baumann, K.; Shaw, S. L.; Guo, H.; King, L.; Weber, R. J.; Neff, M. E.; Stone, E. A.; Offenberg, J. H.; Zhang, Z.; Gold, A.; Surratt, J. D. Assessing the Impact of Anthropogenic Pollution on Isoprene-Derived Secondary Organic Aerosol Formation in $PM_{2.5}$ Collected from the Birmingham, Alabama, Ground Site during the 2013 Southern Oxidant and Aerosol Study. *Atmos. Chem. Phys.* **2016**, *16* (8), 4897−4914.
(30) Wang, Y.; Zhang, Y.; Li, W.; Wu, G.; Qi, Y.; Li, S.; Zhu, W.; Yu, J. Z.; Yu, X.; Zhang, H.-H.; Sun, J.; Wang, W.; Sheng, L.; Yao, X.; Gao, H.; Huang, C.; Ma, Y.; Zhou, Y. Important Roles and Formation of Atmospheric Organosulfates in Marine Organic Aerosols: Influence of Phytoplankton Emissions and Anthropogenic Pollutants. *Environ. Sci. Technol.* **2023**, *57* (28), 10284−10294.
(31) Huang, R.-J.; Cao, J.; Chen, Y.; Yang, L.; Shen, J.; You, Q.; Wang, K.; Lin, C.; Xu, W.; Gao, B.; Li, Y.; Chen, Q.; Hoffmann, T.; O'Dowd, C. D.; Bilde, M.; Glasius, M. Organosulfates in Atmospheric Aerosol: Synthesis and Quantitative Analysis of $PM_{2.5}$ from Xi'an, Northwestern China. *Atmos. Meas. Tech.* **2018**, *11* (6), 3447−3456.
(32) Ding, S.; Chen, Y.; Devineni, S. R.; Pavuluri, C. M.; Li, X.-D. Distribution Characteristics of Organosulfates (OSs) in $PM_{2.5}$ in Tianjin, Northern China: Quantitative Analysis of Total and Three OS Species. *Sci. Total Environ.* **2022**, *834*, No. 155314.
(33) Liao, J.; Froyd, K. D.; Murphy, D. M.; Keutsch, F. N.; Yu, G.; Wennberg, P. O.; St Clair, J. M.; Crounse, J. D.; Wisthaler, A.; Mikoviny, T.; Jimenez, J. L.; Campuzano-Jost, P.; Day, D. A.; Hu, W.; Ryerson, T. B.; Pollack, I. B.; Peischl, J.; Anderson, B. E.; Ziemba, L. D.; Blake, D. R.; Meinardi, S.; Diskin, G. Airborne Measurements of Organosulfates over the Continental U.S. *J. Geophys. Res.: Atmos.* **2015**, *120* (7), 2990−3005.
(34) Wang, Y.; Liang, S.; Le Breton, M.; Wang, Q. Q.; Liu, Q.; Ho, C. H.; Kuang, B. Y.; Wu, C.; Hallquist, M.; Tong, R.; Yu, J. Z. Field Observations of C_2 and C_3 Organosulfates and Insights into Their Formation Mechanisms at a Suburban Site in Hong Kong. *Sci. Total Environ.* **2023**, *904*, No. 166851.
(35) Passananti, M.; Kong, L.; Shang, J.; Dupart, Y.; Perrier, S.; Chen, J.; Donaldson, D. J.; George, C. Organosulfate Formation through the Heterogeneous Reaction of Sulfur Dioxide with Unsaturated Fatty Acids and Long-Chain Alkenes. *Angew. Chem., Int. Ed.* **2016**, *55* (35), 10336−10339.
(36) Ehn, M.; Junninen, H.; Petäjä, T.; Kurtén, T.; Kerminen, V. M.; Schobesberger, S.; Manninen, H. E.; Ortega, I. K.; Vehkamäki, H.; Kulmala, M.; Worsnop, D. R. Composition and Temporal Behavior of Ambient Ions in the Boreal Forest. *Atmos. Chem. Phys.* **2010**, *10* (17), 8513−8530.
(37) Ye, C.; Yuan, B.; Lin, Y.; Wang, Z.; Hu, W.; Li, T.; Chen, W.; Wu, C.; Wang, C.; Huang, S.; Qi, J.; Wang, B.; Wang, C.; Song, W.; Wang, X.; Zheng, E.; Krechmer, J. E.; Ye, P.; Zhang, Z.; Wang, X.; Worsnop, D. R.; Shao, M. Chemical Characterization of Oxygenated Organic Compounds in the Gas Phase and Particle Phase Using Iodide CIMS with FIGAERO in Urban Air. *Atmos. Chem. Phys.* **2021**, *21* (11), 8455−8478.
(38) Le Breton, M.; Wang, Y.; Hallquist, Å. M.; Pathak, R. K.; Zheng, J.; Yang, Y.; Shang, D.; Glasius, M.; Bannan, T. J.; Liu, Q.; Chan, C. K.; Percival, C. J.; Zhu, W.; Lou, S.; Topping, D.; Wang, Y.; Yu, J.; Lu, K.; Guo, S.; Hu, M.; Hallquist, M. Online Gas- and Particle-Phase Measurements of Organosulfates, Organosulfonates and Nitrooxy Organosulfates in Beijing Utilizing a FIGAERO ToF-CIMS. *Atmos. Chem. Phys.* **2018**, *18* (14), 10355−10371.
(39) Li, L.; Zhang, Q.; Wei, Y.; Wang, Q.; Wang, W. Theoretical Study on the Gas Phase and Gas-Liquid Interface Reaction Mechanism of Criegee Intermediates with Glycolic Acid Sulfate. *Int. J. Mol. Sci.* **2023**, *24* (4), 3355.
(40) Zhang, X.; Lian, Y.; Tan, S.; Yin, S. Organosulfate Produced from Consumption of SO_3 Speeds up Sulfuric Acid-Dimethylamine Atmospheric Nucleation. *Atmos. Chem. Phys.* **2024**, *24* (6), 3593−3612.
(41) Liu, Y.; Nie, W.; Xu, Z.; Wang, T.; Wang, R.; Li, Y.; Wang, L.; Chi, X.; Ding, A. Semi-Quantitative Understanding of Source Contribution to Nitrous Acid (HONO) Based on 1 year of Continuous Observation at the Sorpes Station in Eastern China. *Atmos. Chem. Phys.* **2019**, *19* (20), 13289−13308.
(42) Ding, A. J.; Fu, C.; Yang, X.; Sun, J.; Zheng, L.; Xie, Y.; Herrmann, E.; Nie, W.; Petäjä, T.; Kerminen, V.-M.; Kulmala, M. Ozone and Fine Particle in the Western Yangtze River Delta: An Overview of 1 Yr Data at the Sorpes Station. *Atmos. Chem. Phys.* **2013**, *13* (11), 5813−5830.
(43) Qi, X. M.; Ding, A.; Nie, W.; Petäjä, T.; Kerminen, V.-M.; Herrmann, E.; Xie, Y.; Zheng, L.; Manninen, H.; Aalto, P.; Sun, J.; Xu, Z.; Chi, X.; Huang, X.; Boy, M.; Virkkula, A.; Yang, X.; Fu, C.; Kulmala, M. Aerosol Size Distribution and New Particle Formation in the Western Yangtze River Delta of China: 2 Years of Measurements at the Sorpes Station. *Atmos. Chem. Phys.* **2015**, *15* (21), 12445−12464.
(44) Wang, J.; Nie, W.; Cheng, Y.; Shen, Y.; Chi, X.; Wang, J.; Huang, X.; Xie, Y.; Sun, P.; Xu, Z.; Qi, X.; Su, H.; Ding, A. Light Absorption of Brown Carbon in Eastern China Based on 3-Year Multi-Wavelength Aerosol Optical Property Observations and an Improved Absorption Ångström Exponent Segregation Method. *Atmos. Chem. Phys.* **2018**, *18* (12), 9061−9074.
(45) Sun, P.; Nie, W.; Chi, X.; Xie, Y.; Huang, X.; Xu, Z.; Qi, X.; Xu, Z.; Wang, L.; Wang, T.; Zhang, Q.; Ding, A. Two Years of Online Measurement of Fine Particulate Nitrate in the Western Yangtze River Delta: Influences of Thermodynamics and N_2O_5 Hydrolysis. *Atmos. Chem. Phys.* **2018**, *18* (23), 17177−17190.
(46) Jokinen, T.; Sipilä, M.; Junninen, H.; Ehn, M.; Lönn, G.; Hakala, J.; Petäjä, T.; Mauldin, R. L.; Kulmala, M.; Worsnop, D. R. Atmospheric Sulphuric Acid and Neutral Cluster Measurements Using CI-APi-TOF. *Atmos. Chem. Phys.* **2012**, *12* (9), 4117−4125.
(47) Liu, Y.; Nie, W.; Li, Y.; Ge, D.; Liu, C.; Xu, Z.; Chen, L.; Wang, T.; Wang, L.; Sun, P.; Qi, X.; Wang, J.; Xu, Z.; Yuan, J.; Yan, C.; Zhang, Y.; Huang, D.; Wang, Z.; Donahue, N. M.; Worsnop, D.; Chi, X.; Ehn, M.; Ding, A. Formation of Condensable Organic Vapors from Anthropogenic and Biogenic Volatile Organic Compounds (VOCs) Is Strongly Perturbed by NO_x in Eastern China. *Atmos. Chem. Phys.* **2021**, *21* (19), 14789−14814.
(48) Liu, Y.; Liu, C.; Nie, W.; Li, Y.; Ge, D.; Chen, L.; Zhu, C.; Wang, L.; Zhang, Y.; Liu, T.; Qi, X.; Wang, J.; Huang, D.; Wang, Z.; Yan, C.; Chi, X.; Ding, A. Exploring Condensable Organic Vapors and Their Co-Occurrence with $PM_{2.5}$ and O_3 in Winter in Eastern China. *Environ. Sci.: Atmos.* **2023**, *3* (2), 282−297.
(49) Liu, Y.; Nie, W.; Qi, X.; Li, Y.; Xu, T.; Liu, C.; Ge, D.; Chen, L.; Niu, G.; Wang, J.; Yang, L.; Wang, L.; Zhu, C.; Wang, J.; Zhang, Y.; Liu, T.; Zha, Q.; Yan, C.; Ye, C.; Zhang, G.; Hu, R.; Huang, R.; Chi, X.; Zhu, T.; Ding, A. The Pivotal Role of Heavy Terpenes and Anthropogenic Interactions in New Particle Formation on the Southeastern Qinghai-Tibet Plateau. *Environ. Sci. Technol.* **2024**, *58* (44), 19748−19761.
(50) Kürten, A.; Rondo, L.; Ehrhart, S.; Curtius, J. Calibration of a Chemical Ionization Mass Spectrometer for the Measurement of Gaseous Sulfuric Acid. *J. Phys. Chem. A* **2012**, *116* (24), 6375−6386.
(51) Alage, S.; Michoud, V.; Harb, S.; Picquet-Varrault, B.; Cirtog, M.; Kumar, A.; Rissanen, M.; Cantrell, C. A Nitrate Ion Chemical-Ionization Atmospheric-Pressure-Interface Time-of-Flight Mass Spectrometer (NO_3^- ToFCIMS) Sensitivity Study. *Atmos. Meas. Tech.* **2024**, *17* (15), 4709−4724.
(52) Lopez-Hilfiker, F. D.; Mohr, C.; Ehn, M.; Rubach, F.; Kleist, E.; Wildt, J.; Mentel, T. F.; Lutz, A.; Hallquist, M.; Worsnop, D.; Thornton, J. A. A Novel Method for Online Analysis of Gas and Particle Composition: Description and Evaluation of a Filter Inlet for Gases and Aerosols (FIGAERO). *Atmos. Meas. Tech.* **2014**, *7* (4), 983−1001.
(53) Ehn, M.; Thornton, J. A.; Kleist, E.; Sipilä, M.; Junninen, H.; Pullinen, I.; Springer, M.; Rubach, F.; Tillmann, R.; Lee, B.; Lopez-Hilfiker, F.; Andres, S.; Acir, I.-H.; Rissanen, M.; Jokinen, T.; Schobesberger, S.; Kangasluoma, J.; Kontkanen, J.; Nieminen, T.;

Kurtén, T.; Nielsen, L. B.; Jørgensen, S.; Kjaergaard, H. G.; Canagaratna, M.; Maso, M. D.; Berndt, T.; Petäjä, T.; Wahner, A.; Kerminen, V.-M.; Kulmala, M.; Worsnop, D. R.; Wildt, J.; Mentel, T. F. A Large Source of Low-Volatility Secondary Organic Aerosol. *Nature* **2014**, *506* (7489), 476−479.
(54) Bannan, T. J.; Le Breton, M.; Priestley, M.; Worrall, S. D.; Bacak, A.; Marsden, N. A.; Mehra, A.; Hammes, J.; Hallquist, M.; Alfarra, M. R.; Krieger, U. K.; Reid, J. P.; Jayne, J.; Robinson, W.; McFiggans, G.; Coe, H.; Percival, C. J.; Topping, D. A Method for Extracting Calibrated Volatility Information from the FIGAERO-HR-ToF-CIMS and Its Experimental Application. *Atmos. Meas. Tech.* **2019**, *12* (3), 1429−1439.
(55) Ylisirniö, A.; Buchholz, A.; Mohr, C.; Li, Z.; Barreira, L.; Lambe, A.; Faiola, C.; Kari, E.; Yli-Juuti, T.; Nizkorodov, S. A.; Worsnop, D. R.; Virtanen, A.; Schobesberger, S. Composition and Volatility of Secondary Organic Aerosol (SOA) Formed from Oxidation of Real Tree Emissions Compared to Simplified Volatile Organic Compound (VOC) Systems. *Atmos. Chem. Phys.* **2020**, *20* (9), 5629−5644.
(56) Ren, S.; Yao, L.; Wang, Y.; Yang, G.; Liu, Y.; Li, Y.; Lu, Y.; Wang, L.; Wang, L. Volatility Parameterization of Ambient Organic Aerosols at a Rural Site of the North China Plain. *Atmos. Chem. Phys.* **2022**, *22* (14), 9283−9297.
(57) Pankow, J. F. An Absorption Model of Gas/Particle Partitioning of Organic Compounds in the Atmosphere. *Atmos. Environ.* **1994**, *28* (2), 185−188.
(58) Lopez-Hilfiker, F. D.; Mohr, C.; Ehn, M.; Rubach, F.; Kleist, E.; Wildt, J.; Mentel, T. F.; Carrasquillo, A. J.; Daumit, K. E.; Hunter, J. F.; Kroll, J. H.; Worsnop, D. R.; Thornton, J. A. Phase Partitioning and Volatility of Secondary Organic Aerosol Components Formed from α-Pinene Ozonolysis and OH Oxidation: The Importance of Accretion Products and Other Low Volatility Compounds. *Atmos. Chem. Phys.* **2015**, *15* (14), 7765−7776.
(59) Mochizuki, T.; Kawamura, K.; Nakamura, S.; Kanaya, Y.; Wang, Z. Enhanced Levels of Atmospheric Low-Molecular Weight Monocarboxylic Acids in Gas and Particulates over Mt. Tai, North China, during Field Burning of Agricultural Wastes. *Atmos. Environ.* **2017**, *171*, 237−247.
(60) Stieger, B.; van Pinxteren, D.; Tilgner, A.; Spindler, G.; Poulain, L.; Grüner, A.; Wallasch, M.; Herrmann, H. Strong Deviations from Thermodynamically Expected Phase Partitioning of Low-Molecular-Weight Organic Acids during One Year of Rural Measurements. *ACS Earth Space Chem.* **2021**, *5* (3), 500−515.
(61) Zhou, C.; Jang, M.; Yu, Z. Simulation of SOA Formation from the Photooxidation of Monoalkylbenzenes in the Presence of Aqueous Aerosols Containing Electrolytes under Various NO_x Levels. *Atmos. Chem. Phys.* **2019**, *19* (8), 5719−5735.
(62) Churchill, B.; Acree, W. E.; Abraham, M. H. Development of Abraham Model Expressions for Predicting the Standard Molar Enthalpies of Vaporization of Organic Compounds at 298.15 K. *Thermochim. Acta* **2019**, *681*, No. 178372.
(63) Long, B.; Xia, Y.; Zhang, Y.-Q.; Truhlar, D. G. Kinetics of Sulfur Trioxide Reaction with Water Vapor to Form Atmospheric Sulfuric Acid. *J. Am. Chem. Soc.* **2023**, *145* (36), 19866−19876.
(64) Yang, L.; Nie, W.; Liu, Y.; Xu, Z.; Xiao, M.; Qi, X.; Li, Y.; Wang, R.; Zou, J.; Paasonen, P.; Yan, C.; Xu, Z.; Wang, J.; Zhou, C.; Yuan, J.; Sun, J.; Chi, X.; Kerminen, V.-M.; Kulmala, M.; Ding, A. Toward Building a Physical Proxy for Gas-Phase Sulfuric Acid Concentration Based on Its Budget Analysis in Polluted Yangtze River Delta, East China. *Environ. Sci. Technol.* **2021**, *55* (10), 6665−6676.
(65) Wang, Z.; Nie, W.; Liu, Y.; Yang, L.; Liu, C.; Zhang, Y.; Yan, C.; Zha, Q.; Ge, D.; Qi, X.; Zhou, C.; Chen, L.; Zhou, X.; Wang, L.; Huang, D. D.; Chi, X.; Ding, A. Gaseous Sulfuric Acid Contributions to Sulfate Formation in Urban Atmosphere. *Environ. Sci. Technol.* **2025**, *12* (2), 189−195.
(66) Stark, H.; Yatavelli, R. L. N.; Thompson, S. L.; Kang, H.; Krechmer, J. E.; Kimmel, J. R.; Palm, B. B.; Hu, W.; Hayes, P. L.; Day, D. A.; Campuzano-Jost, P.; Canagaratna, M. R.; Jayne, J. T.; Worsnop, D. R.; Jimenez, J. L. Impact of Thermal Decomposition on Thermal Desorption Instruments: Advantage of Thermogram Analysis for Quantifying Volatility Distributions of Organic Species. *Environ. Sci. Technol.* **2017**, *51* (15), 8491−8500.
(67) Nozière, B.; Kalberer, M.; Claeys, M.; Allan, J.; D'Anna, B.; Decesari, S.; Finessi, E.; Glasius, M.; Grgić, I.; Hamilton, J. F.; Hoffmann, T.; Iinuma, Y.; Jaoui, M.; Kahnt, A.; Kampf, C. J.; Kourtchev, I.; Maenhaut, W.; Marsden, N.; Saarikoski, S.; Schnelle-Kreis, J.; Surratt, J. D.; Szidat, S.; Szmigielski, R.; Wisthaler, A. The Molecular Identification of Organic Compounds in the Atmosphere: State of the Art and Challenges. *Chem. Rev.* **2015**, *115* (10), 3919−3983.
(68) Ylisirniö, A.; Barreira, L. M. F.; Pullinen, I.; Buchholz, A.; Jayne, J.; Krechmer, J. E.; Worsnop, D. R.; Virtanen, A.; Schobesberger, S. On the Calibration of FIGAERO-ToF-CIMS: Importance and Impact of Calibrant Delivery for the Particle-Phase Calibration. *Atmos. Meas. Tech.* **2021**, *14* (1), 355−367.
(69) Hyttinen, N.; Pullinen, I.; Nissinen, A.; Schobesberger, S.; Virtanen, A.; Yli-Juuti, T. Comparison of Saturation Vapor Pressures of α-Pinene + O_3 Oxidation Products Derived from COSMO-RS Computations and Thermal Desorption Experiments. *Atmos. Chem. Phys.* **2022**, *22* (2), 1195−1208.
(70) Cai, M.; Ye, C.; Yuan, B.; Huang, S.; Zheng, E.; Yang, S.; Wang, Z.; Lin, Y.; Li, T.; Hu, W.; Chen, W.; Song, Q.; Li, W.; Peng, Y.; Liang, B.; Sun, Q.; Zhao, J.; Chen, D.; Sun, J.; Yang, Z.; Shao, M. Enhanced Daytime Secondary Aerosol Formation Driven by Gas-Particle Partitioning in Downwind Urban Plumes. *Atmos. Chem. Phys.* **2024**, *24* (22), 13065−13079.
(71) Voliotis, A.; Wang, Y.; Shao, Y.; Du, M.; Bannan, T. J.; Percival, C. J.; Pandis, S. N.; Alfarra, M. R.; McFiggans, G. Exploring the Composition and Volatility of Secondary Organic Aerosols in Mixed Anthropogenic and Biogenic Precursor Systems. *Atmos. Chem. Phys.* **2021**, *21* (18), 14251−14273.
(72) Donahue, N. M.; Robinson, A. L.; Pandis, S. N. Atmospheric Organic Particulate Matter: From Smoke to Secondary Organic Aerosol. *Atmos. Environ.* **2009**, *43* (1), 94−106.
(73) Schervish, M.; Donahue, N. M. Peroxy Radical Chemistry and the Volatility Basis Set. *Atmos. Chem. Phys.* **2020**, *20* (2), 1183−1199.
(74) Huang, W.; Li, H.; Sarnela, N.; Heikkinen, L.; Tham, Y. J.; Mikkilä, J.; Thomas, S. J.; Donahue, N. M.; Kulmala, M.; Bianchi, F. Measurement Report: Molecular Composition and Volatility of Gaseous Organic Compounds in a Boreal Forest - from Volatile Organic Compounds to Highly Oxygenated Organic Molecules. *Atmos. Chem. Phys.* **2021**, *21* (11), 8961−8977.
(75) Tröstl, J.; Chuang, W. K.; Gordon, H.; Heinritzi, M.; Yan, C.; Molteni, U.; Ahlm, L.; Frege, C.; Bianchi, F.; Wagner, R.; Simon, M.; Lehtipalo, K.; Williamson, C.; Craven, J. S.; Duplissy, J.; Adamov, A.; Almeida, J.; Bernhammer, A.-K.; Breitenlechner, M.; Brilke, S.; Dias, A.; Ehrhart, S.; Flagan, R. C.; Franchin, A.; Fuchs, C.; Guida, R.; Gysel, M.; Hansel, A.; Hoyle, C. R.; Jokinen, T.; Junninen, H.; Kangasluoma, J.; Keskinen, H.; Kim, J.; Krapf, M.; Kürten, A.; Laaksonen, A.; Lawler, M.; Leiminger, M.; Mathot, S.; Möhler, O.; Nieminen, T.; Onnela, A.; Petäjä, T.; Piel, F. M.; Miettinen, P.; Rissanen, M. P.; Rondo, L.; Sarnela, N.; Schobesberger, S.; Sengupta, K.; Sipilä, M.; Smith, J. N.; Steiner, G.; Tomè, A.; Virtanen, A.; Wagner, A. C.; Weingartner, E.; Wimmer, D.; Winkler, P. M.; Ye, P.; Carslaw, K. S.; Curtius, J.; Dommen, J.; Kirkby, J.; Kulmala, M.; Riipinen, I.; Worsnop, D. R.; Donahue, N. M.; Baltensperger, U. The Role of Low-Volatility Organic Compounds in Initial Particle Growth in the Atmosphere. *Nature* **2016**, *533* (7604), 527−531.
(76) Liu, L.; Zhong, J.; Vehkamäki, H.; Kurtén, T.; Du, L.; Zhang, X.; Francisco, J. S.; Zeng, X. C. Unexpected Quenching Effect on New Particle Formation from the Atmospheric Reaction of Methanol with SO_3. *Proc. Natl. Acad. Sci. U.S.A.* **2019**, *116* (50), 24966−24971.
(77) Kumar, A.; Iyer, S.; Barua, S.; Brean, J.; Besic, E.; Seal, P.; Dall'Osto, M.; Beddows, D. C. S.; Sarnela, N.; Jokinen, T.; Sipilä, M.; Harrison, R. M.; Rissanen, M. Direct Measurements of Covalently Bonded Sulfuric Anhydrides from Gas-Phase Reactions of SO_3 with Acids under Ambient Conditions. *J. Am. Chem. Soc.* **2024**, *146* (22), 15562−15575.

(78) Friedman, B.; Brophy, P.; Brune, W. H.; Farmer, D. K. Anthropogenic Sulfur Perturbations on Biogenic Oxidation: SO_2 Additions Impact Gas-Phase OH Oxidation Products of α- and β-Pinene. *Environ. Sci. Technol.* **2016**, *50* (3), 1269−1279.
(79) Kirkby, J.; Duplissy, J.; Sengupta, K.; Frege, C.; Gordon, H.; Williamson, C.; Heinritzi, M.; Simon, M.; Yan, C.; Almeida, J.; Tröstl, J.; Nieminen, T.; Ortega, I. K.; Wagner, R.; Adamov, A.; Amorim, A.; Bernhammer, A.-K.; Bianchi, F.; Breitenlechner, M.; Brilke, S.; Chen, X.; Craven, J.; Dias, A.; Ehrhart, S.; Flagan, R. C.; Franchin, A.; Fuchs, C.; Guida, R.; Hakala, J.; Hoyle, C. R.; Jokinen, T.; Junninen, H.; Kangasluoma, J.; Kim, J.; Krapf, M.; Kürten, A.; Laaksonen, A.; Lehtipalo, K.; Makhmutov, V.; Mathot, S.; Molteni, U.; Onnela, A.; Peräkylä, O.; Piel, F.; Petäjä, T.; Praplan, A. P.; Pringle, K.; Rap, A.; Richards, N. A. D.; Riipinen, I.; Rissanen, M. P.; Rondo, L.; Sarnela, N.; Schobesberger, S.; Scott, C. E.; Seinfeld, J. H.; Sipilä, M.; Steiner, G.; Stozhkov, Y.; Stratmann, F.; Tomé, A.; Virtanen, A.; Vogel, A. L.; Wagner, A. C.; Wagner, P. E.; Weingartner, E.; Wimmer, D.; Winkler, P. M.; Ye, P.; Zhang, X.; Hansel, A.; Dommen, J.; Donahue, N. M.; Worsnop, D. R.; Baltensperger, U.; Kulmala, M.; Carslaw, K. S.; Curtius, J. Ion-Induced Nucleation of Pure Biogenic Particles. *Nature* **2016**, *533* (7604), 521−526.

https://doi.org/10.1021/acs.est.5c07888
Environ. Sci. Technol. 2025, 59, 16556−16566